AIAA JOURNAL
Vol. 37, No. 7, July 1999

Validation of an Impedance Eduction Method in Flow

Willie R. Watson,* Michael G. Jones,† and Tony L. Parrott‡
NASA Langley Research Center, Hampton, Virginia 23681-0001

Results are reported for validating a method for educing the normal incidence impedance of a locally reacting liner in a grazing incidence, nonprogressive acoustic wave environment with flow. The results demonstrate the ability of the method to reproduce the normal incidence admittance of a solid steel plate and normal incidence impedance of two soft test liners in a uniform flow. The selected test liners are known to be locally reacting and exhibit no amplitude-dependent impedance nonlinearities and only minimal flow effects. Baseline results for these liners are, therefore, established from measurements in a conventional normal incidence impedance tube. A key feature of the method is the expansion of the unknown impedance function as a piecewise continuous polynomial with undetermined coefficients. Stewart's adaptation (Stewart, G. W., III, "A Modification of Davidon's Minimization Method to Accept Difference Approximations of Derivatives," *Journal of ACM*, Vol. 14, No. 1, 1967, pp. 72–83) of the Davidon–Fletcher–Powell optimization algorithm is used to educe the normal incidence impedance at each Mach number by optimizing an objective function. The method very nearly reproduces the normal incidence impedance spectrum for each of the test liners; thus, its usefulness for determining the normal incidence impedance of test liners for a broad range of source frequencies and flow Mach numbers is demonstrated.

Nomenclature

$[A_I]$, $[B_I]$, $[C_I]$	= major blocks in $[A(\beta_{Iq})]$
$[A^{[I,J]}]$	= local element matrix
$[A(\beta_{Iq})]$, $[AB]$	= block-tridiagonal matrices
a, b	= length and height of an element
$[a_I]$, $[b_I]$, $[c_I]$	= minor blocks in $[A(\beta_{Iq})]$
c_0, ρ_0	= ambient sound speed and density
dA	= differential of cross-sectional area
$E(x, y)$	= field-equation error function
$\{F\}$	= vector that contains source effects
$f_q(x)$, $N_I(x, y)$	= one- and two-dimensional basis functions, respectively
H, L	= height and length of duct
i	= $\sqrt{-1}$
k	= free-space wave number, ω/c_0
L_1, L_2	= leading and trailing edge of liner
M, N	= total number of transverse and axial nodes
M_0	= average flow Mach number, u_0/c_0
m	= number of upper wall measurement points
$p(x, y)$	= acoustic pressure at (x, y)
$p_{FE}(x_l; \beta_{Iq})$	= finite element wall pressure
$p_s(y)$, p_{ref}	= source and reference pressure
$SPL(x_l)$	= upper wall sound pressure level
u, v	= axial and transverse velocity
u_0	= flow speed in axial direction
x, y, z	= Cartesian coordinates
x_l	= upper wall measurement location
β_{Iq}	= admittance coefficient determined from optimized objective function
$\beta(x)$	= normalized wall admittance, $1/\zeta(x)$
$\zeta(x)$, $\zeta_{exit}(y)$	= wall and exit impedance, normalized with $\rho_0 c_0$
θ, χ	= resistance and reactance
κ, σ	= conductance and susceptance
Φ_I	= nodal value of acoustic pressures
$\{\Phi\}$	= global vector of acoustic pressures
$\{\Phi^{[I,J]}\}$	= local vector of acoustic pressures
$\phi(x_l)$	= relative phase
$\psi(\beta_{Iq})$	= objective function
ω	= angular frequency
$\|\ \|$	= absolute value

Subscripts

I, J	= node counters for axial and transverse directions of duct
m	= number of wall measurement points
q	= $1, \ldots, 4$

Superscript

T	= matrix transposition

Introduction

EFFICIENT duct treatments for broadband acoustic noise suppression remain critical to the development of environmentally acceptable commercial aircraft in the next century. To this end, an accurate knowledge of duct-treatment impedance is imperative. Validation of liner impedance prediction models for grazing flow is commonly accomplished in a flow duct that provides grazing flow/grazing-incidence sound on a test liner. From appropriate measurements, the normal incidence impedance in a grazing-incidence and grazing flow environment and for locally reacting test materials can, in theory, be educed. Depending on the accuracy/precision required, several methods or approaches are available for accomplishing this eduction process. The simplest approach, the so-called infinite-waveguide method, relies on the measurement of the propagation constant of an assumed single, unidirectional propagating mode[1–3] that is directly related to the normal incidence impedance of the test specimen by means of a modal solution. In real facilities, sufficiently idealized test conditions, i.e., a unidirectional, single propagating mode, are rarely attained. Additionally, if the test liner impedance is nonuniform or the flow Mach number is sufficiently high, added wave field complexity can result either from energy scattering into higher-order modes or from end reflections. Although these conditions may be desirable for achieving more efficient, broadband absorbing structures, they are complicating features that cannot be handled by the infinite-waveguide method for impedance determination.

Received 4 May 1998; presented as Paper 98-2279 at the AIAA/CEAS 4th Aeroacoustics Conference, Toulouse, France, 2–4 June 1998; revision received 11 January 1999; accepted for publication 22 January 1999.

*Senior Research Scientist, Aero and Acoustics Methods Branch, Fluid Mechanics and Acoustics Division.

†Research Scientist, Structural Acoustics Branch, Fluid Mechanics and Acoustics Division.

‡Senior Research Scientist, Structural Acoustics Branch, Fluid Mechanics and Acoustics Division.

Two recent papers presented results from a finite element-based contour deformation method[4,5] for educing the uniform impedance of an acoustic material located in a no-flow duct carrying a nonprogressive multimodal sound field. The contour deformation method was replaced by a more efficient optimization algorithm, and the method was extended and validated for variable impedance liners.[6] To continue to increase the realism of this validation process, the next step is to incorporate flow effects.

The purposes of this paper are to extend the impedance eduction method[6] to include the convective effects of a flow and to perform a validation exercise. The successful validation of an impedance eduction method contains two elements. The first element requires agreement for linear liners between impedance values educed in the presence of flow and those educed at normal incidence with no flow. The second element of a successful validation exercise requires accurate eduction of impedance values for nonlinear liners at various sound pressure levels (SPLs) and mean flow rates. The validation discussed in this study will focus on the first element. To accomplish this goal, special care is taken to choose test liners that are demonstrably locally reacting, for which the normal incidence impedance exhibits no measurable amplitude-dependent behavior and for which the convective effects of the grazing flow are minimal.

Problem Description

The two-dimensional test region shown in Fig. 1 is spanned by x and y coordinates. The region is L units long, with the source and exit planes at $x=0$ and L, respectively. Note that the MKS system of measurement is used throughout this paper. Measured inputs at the source and exit planes are the source pressure $p_s(y)$ and the exit impedance $\zeta_{\text{exit}}(y)$, respectively. A total of m points are located at $x=x_1, x_2, x_3, \ldots, x_m$ along the rigid upper wall, at which the complex acoustic pressures are measured. The test liner is the part of the otherwise rigid bottom wall between $L_1 \le x \le L_2$. The lining material has an unknown impedance distribution $\zeta(x)$, as shown. The uniform flow, of speed u_0, is subsonic and flows from left to right. The problem is to determine the impedance of the material as a function of the flow Mach number from the measured boundary data.

Steady-state acoustic pressure waves that propagate within the duct shown in Fig. 1 satisfy the equations[7]

$$i\omega p + u_0\frac{\partial p}{\partial x} = -\rho_0 c_0^2\left(\frac{\partial u}{\partial x}+\frac{\partial v}{\partial y}\right) \tag{1}$$

$$i\omega u + u_0\frac{\partial u}{\partial x} = -\frac{1}{\rho_0}\frac{\partial p}{\partial x} \tag{2}$$

$$i\omega v + u_0\frac{\partial v}{\partial x} = -\frac{1}{\rho_0}\frac{\partial p}{\partial y} \tag{3}$$

Physically, these three continuity equations represent the linearized conservation equations for mass, axial momentum, and transverse momentum, respectively, in the flowing fluid. Equations (1–3) are conveniently combined into a single second-order partial differential equation on the acoustic pressure field:

$$\left(1-M_0^2\right)\frac{\partial^2 p}{\partial x^2}+\frac{\partial^2 p}{\partial y^2}-2ikM_0\frac{\partial p}{\partial x}+k^2 p=0 \tag{4}$$

Before a solution to the acoustic field can be obtained and the unknown impedance educed, boundary conditions must be prescribed.

Along the source plane of the duct ($x=0$), the acoustic pressure $p_s(y)$ is assumed to be measured as

$$p = p_s \tag{5}$$

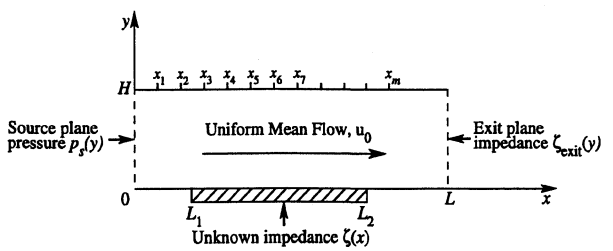

Fig. 1 Two-dimensional duct and coordinate system.

Along the rigid upper wall, the normal component of acoustic particle velocity must vanish, i.e., $v=0$; thus,

$$\frac{\partial p}{\partial y}=0 \tag{6}$$

At the duct termination ($x=L$), the ratio of the acoustic pressure to the normal component of acoustic particle velocity must equal the measured exit impedance $\zeta_{\text{exit}}(y)$:

$$p/u = \zeta_{\text{exit}} \tag{7}$$

which when substituted into the axial momentum equation (2) and simplified gives

$$\frac{\partial p}{\partial x}=\frac{-ikp}{[M_0+\zeta_{\text{exit}}]} \tag{8}$$

The lower wall, locally reacting condition gives[8]

$$vic_0k = -\beta p - \frac{M_0}{ik}\frac{\partial}{\partial x}[\beta p] \tag{9}$$

when expressed in terms of $\beta(x)$, the reciprocal of the impedance function. Equation (9) can be conveniently substituted into the transverse momentum equation (3) to yield

$$\frac{\partial p}{\partial y} = ik\beta p + 2M_0\frac{\partial}{\partial x}[\beta p] + \frac{M_0^2}{ik}\frac{\partial^2}{\partial x^2}[\beta p] \tag{10}$$

Equations (4–6), (8), and (10) form a boundary-value problem that can be solved numerically to determine the upper wall pressures for a given admittance function $\beta(x)$. Conversely, if the upper wall pressures at $x=x_1, x_2, x_3, \ldots, x_m$ are measured along with $p_s(y)$, $p(x, H)$, and $\zeta_{\text{exit}}(y)$, then a unique test liner impedance function exists that will reproduce these wall pressures. Thus, the goal of this paper is to devise a procedure for educing this unknown liner impedance function from measured complex acoustic pressures.

Numerical Method

The numerical method chosen to solve the governing equation coupled with the boundary conditions is the finite element method. The finite element methodology closely parallels that used in an earlier paper.[4] When applied to the current acoustic problem, the finite element method may be interpreted as an approximation to the continuous acoustic field as an assemblage of rectangular elements (Fig. 2). Here, N nodes are assumed in the axial direction of the duct and M nodes are assumed in the transverse direction of the duct. A typical rectangular element with width a and height b (Fig. 3) consists of four local node numbers, labeled 1, 2, 3, and 4, respectively. The objective is to obtain the unknown acoustic pressures at the nodes of each of the $(M-1)(N-1)$ elements. Galerkin's finite element method is used to minimize the field error. The field error function is defined as

$$E(x,y)=\left(1-M_0^2\right)\frac{\partial^2 p}{\partial x^2}+\frac{\partial^2 p}{\partial y^2}-2ikM_0\frac{\partial p}{\partial x}+k^2 p \tag{11}$$

Within each element, the acoustic pressure p is expanded as a series:

$$p(x,y)=\sum_{I=1}^{NDOF} N_I(x,y)\Phi_I \tag{12}$$

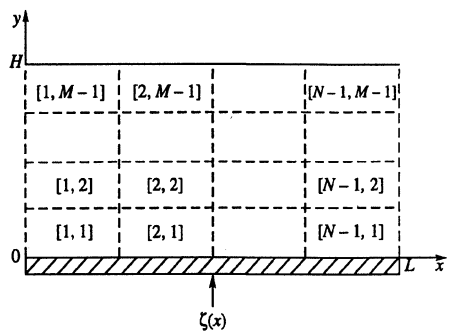

Fig. 2 Finite element discretization of two-dimensional duct.

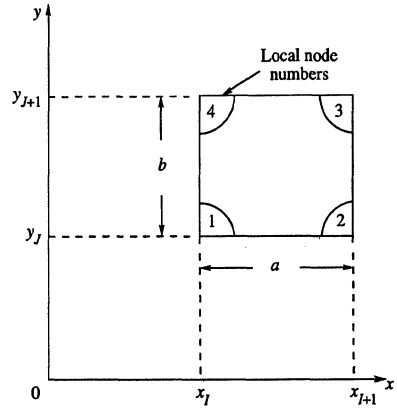

Fig. 3 Typical finite element and local node numbering system.

where $N\text{DOF}$, $N_I(x, y)$, and Φ_I are the number of degrees of freedom (DOF), the basis functions, and nodal coefficients, respectively, for the element.

In the earlier paper[4] on no flow, linear basis functions were used, and the nodal coefficients were the acoustic pressures at the four nodes of the element. However, the convective effects of the flow have introduced second-derivative terms in the wall admittance boundary condition (10), so that the basis functions used in the finite element method must be such that both the acoustic pressure p and its axial derivative are continuous at the lower boundary. The lowest-order, fully compatible, rectangular element satisfying these two continuity conditions is that used for plate bending.[9] The plate bending element was introduced over three decades ago and has been used successfully in both structural analysis[9] and nacelle acoustics.[10] A typical plate bending element consists of 16, i.e., $N\text{DOF} = 16$, cubic Hermite polynomials $N_I(x, y)$ and nodal coefficients Φ_I (Ref. 9). Expressions for the nodal coefficient Φ_I and basis function $N_I(x, y)$ for a typical plate bending element are rather lengthy and are not written explicitly in this paper because they can be found elsewhere.[9]

The variable exit impedance $\zeta_{\text{exit}}(y)$ and wall admittance $\beta(x)$ are also represented in terms of series along each boundary element:

$$\zeta_{\text{exit}}(y) = \zeta_{\text{exit}}(y_J) f_1(y) + \zeta_{\text{exit}}(y_{J+1}) f_3(y) + \zeta'_{\text{exit}}(y_J) f_2(y) + \zeta'_{\text{exit}}(y_{J+1}) f_4(y) \tag{13}$$

$$\beta(x) = \beta_{I1} f_1(x) + \beta_{I2} f_2(x) + \beta_{I3} f_3(x) + \beta_{I4} f_4(x) \tag{14}$$

where β_{Iq} are unknown coefficients to be determined and f_I are the one-dimensional Hermite polynomials for plate bending.[9] For $(N-1)$ columns of elements, $4(N-1)$ coefficients must be determined. Ideally, the solution to the sound field is obtained when the field error $E(x, y)$ is identically zero at each point of the domain. Thus, the field error function is made to be orthogonal to each basis function $N_I(x, y)$. Contributions to the minimization of the field error function from a typical element are

$$\int E N_I \, dA \tag{15}$$

Each second-derivative term in the integrand of Eq. (15) is integrated by parts, and the admittance boundary conditions are incorporated at the element level as in Ref. 4.

The contribution to the minimization of the field error for each element is expressed in matrix form as

$$\int E N_I \, dA = \left[A^{[I,J]}\right]\left\{\Phi^{[I,J]}\right\} \tag{16}$$

where $[A^{[I,J]}]$ is a 16×16 complex matrix for each element $[I, J]$ and $\{\Phi^{[I,J]}\}$ is a 16×1 column vector that contains the unknown acoustic pressure and its derivatives at the four nodes of the element. The coefficients in the local stiffness matrix $[A^{[I,J]}]$ are computed in closed form.

Assembly of the global equations for the computational domain is a basic procedure in the finite element method. Appropriate shifting of rows and columns is all that is required to add the local element matrix $[A^{[I,J]}]$ directly into the global matrix $[AB]$ (Ref. 9). The elements for the entire domain can be assembled to result in a matrix equation of the form

$$[AB]\{\Phi\} = \{0\} \tag{17}$$

where $[AB]$ is a complex matrix with an order of $4MN$ and $\{\Phi\}$ is a $4MN \times 1$ column vector. The vector $\{\Phi\}$ contains the nodal values of the unknown acoustic pressure and its derivatives at the MN nodes of the duct. The source pressure boundary condition must be applied to this system of equations before a solution can be obtained. To satisfy the noise-source boundary condition, all nodal values of the acoustic pressure at the source plane ($x = 0$) are simply set to the known value of source pressure $p_s(y)$. Thus, after inserting these source conditions into the assembled global matrix equation (17), nonzero elements are introduced into $2M$ components of the zero vector $\{0\}$. This process leads to a modified set of equations of the form

$$[A(\beta_{Iq})]\{\Phi\} = \{F\} \tag{18}$$

The global matrix $[A(\beta_{Iq})]$, which is generated by Galerkin's method, is a complex positive indefinite matrix. The structure of matrix $[A(\beta_{Iq})]$ is as follows:

$$[A(\beta_{Iq})] = \begin{bmatrix} [A_1] & [B_2] & & \\ [C_2] & [A_2] & [B_3] & \\ & \ddots & \ddots & \ddots \\ & & [C_N] & [A_N] \end{bmatrix} \tag{19}$$

Note that $[A(\beta_{Iq})]$ is a square, nonsymmetric block-tridiagonal matrix. This global matrix contains several major blocks, $[A_I]$, $[B_I]$, and $[C_I]$, as shown in Eq. (19). Each major block is a $4M \times 4M$ block-tridiagonal matrix:

$$\begin{bmatrix} [a_1] & [b_2] & & \\ [c_2] & [a_2] & [b_3] & \\ & \ddots & \ddots & \ddots \\ & & [c_M] & [a_M] \end{bmatrix} \tag{20}$$

Each minor block, $[a_J]$, $[b_J]$, and $[c_J]$ is a 4×4 complex matrix so that the order of $[A(\beta_{Iq})]$ is $4NM \times 4NM$. When flow is absent, the diagonal major blocks $[A_I]$ are symmetric, and $[C_I]^T = [B_I]$. Much practical importance arises from this structure because of its convenience for minimizing storage and maximizing computational efficiency. Special matrix techniques exist for a solution of this structure. Gaussian elimination with partial pivoting and equivalent row infinity norm scaling is used to reduce the system to upper triangular form. Backsubstitution is then used to obtain the solution for the acoustic pressure and its derivative at the NM node points. All computations are performed only on the elements within the bandwidth of $[A(\beta_{Iq})]$.

Three sets of boundary data are required in addition to the rigid upper wall condition before the duct propagation model described by Eqs. (18) can uniquely determine the upper wall pressure. The impedance eduction method discussed in the following section makes use of the unique relationship between the measured upper wall pressures $p(x_l, H)$ and the following three sets of data: 1) the source plane pressure $p_s(y)$, 2) the exit plane impedance $\zeta_{\text{exit}}(y)$, and 3) the test liner impedance function $\zeta(x) = 1/\beta(x)$. If any two of the listed values and the upper wall pressures are measured, then the remaining values can be determined. We seek the test liner impedance $\zeta(x)$. This function is determined by measuring the upper wall and source pressures and the exit impedance. These measurements are accomplished in the NASA Langley Research Center Flow Impedance Test Facility.

Data Acquisition

The input data used to educe the impedance of each test specimen are obtained from measurements in the Flow Impedance Test Facility at NASA Langley Research Center. A schematic of the flow impedance tube is provided in Fig. 4. This multiconfigurational

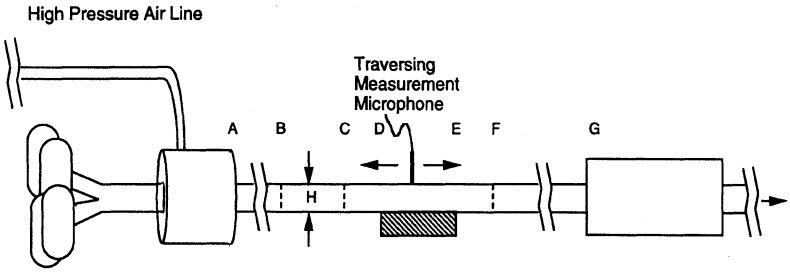

	Distance from source plane , d (m)	Ratio of distance from source plane to duct height, d/H
A - Exit of plenum chamber	-2.34	-46
B - Start of 51x51mm square cross section	-0.94	-16.5
C - Computational source plane	0.00	0
D - Leading edge of acoustic liner	0.20	4
E - Trailing edge of acoustic liner	0.61	12
F - Computational exit plane	0.81	16
G - Entrance to termination section	2.24	44

Fig. 4 Schematic of NASA Langley Research Center flow impedance tube.

apparatus has a 51 × 51 mm cross section in which a controlled aeroacoustic environment can be achieved with a centerline Mach number of up to 0.6 over the test specimen length. The test specimen is centered in a computation domain that runs from a source plane labeled C to an exit plane labeled F.

The desired aeroacoustic environment in the computational domain is achieved with four 120-W acoustic drivers whose phase-matched outputs are converged to a location 2.2 m upstream of the plenum exit by means of a manifold. At the test specimen leading edge, discrete tones with SPLs up to 155 dB can be achieved over a frequency range of 0.3–3.0 kHz. The mean flow is conditioned by a specially designed plenum that allows flow to be combined with the sound field such that sound transmission efficiency degradation is minimal. This is accomplished by equipping the plenum chamber with a porous, inner cylindrical core fabricated of high-flow-resistance fibermetal. The porous cylinder has the same airway cross-sectional area (57-mm inner diameter) as the duct from the acoustic driver manifold. High-pressure air is fed into the coannular region of the plenum and percolates through the porous cylinder walls to combine with the sound from the acoustic drivers. The goal of this mixer design is to minimize the expansion chamber muffling action on the acoustic output from the drivers and also to minimize the introduction of unwanted flow noise.

The combined sound and mean flow exits the plenum chamber into a 57-mm round cross-sectional tube, which extends 0.94 m. A 0.30-m round-to-square tube, which maintains a constant cross-sectional area, is then used to transition to the 51 × 51 mm square test section. The test section (section of the duct between the source and exit plane) is 812 mm long, with the upper and side walls constructed from stainless steel. The sound and flow pass over the liner surface, which forms the lower wall of the duct, and then exit through a termination section, designed to be as nonreflecting as possible.

Throughout the computational domain, three-dimensional mean flow uniformity was assumed (region C–F in Fig. 4). Also, two dimensionality of the acoustic field was maintained as nearly as possible by restricting excitation frequencies to below the 3-kHz cuton in the hardwall region, i.e., only the plane wave propagates in the hardwall region, so that spanwise modes (the source of three-dimensional acoustic effects) were not available to carry a significant amount of acoustic energy.

The leading edge of the test specimen was 50 duct heights downstream of the plenum exit. The Reynolds number range, based on duct height, was from 1.16×10^5 to 5.8×10^5, corresponding to the target centerline Mach numbers of 0.1 and 0.5, respectively. Total-pressure surveys were conducted at three cross-sectional planes located 25, 406, and 787 mm (0.5, 8.0, and 15.5 duct heights) downstream of the source plane, respectively. These surveys were conducted with a 54-port total pressure rake, which was specifically designed for the Flow Impedance Test Facility. Total pressures at each port location were combined with the static pressure, measured in the same axial plane, to determine the mean flow Mach number profile at each axial plane. These same data were also used to determine the mean density, mean pressure, and mean temperature as a function of the flow Mach number. (These flow properties were observed not to change from their ambient values.) On the basis of these profile measurements, the wall boundary layers appear well merged at the source plane. Although the flow profiles were not completely developed in the test section, measurements at the source and exit planes showed little change in profile shape, as evidenced by changes in the ratios of centerline to average velocity of 8 and 5%, respectively, for target centerline Mach numbers of 0.1 and 0.5, respectively. The profiles were observed to follow the $1/N$ power law, with N ranging from 7 to 10 (Ref. 11).

The uniform flow Mach number used to perform each impedance eduction in this report was taken to be the average value of the Mach number profile measured at the midliner axial plane (406 mm downstream of the source plane). Data were taken at four target centerline Mach numbers, i.e., 0.0, 0.1, 0.3, and 0.5. Turbulence levels in the test section were not measured. However, narrowband (1-Hz) flow noise spectra have been measured over the frequency range 0.5–3.0 kHz with the acoustic drivers disengaged.[12] These data showed that at a centerline Mach number of 0.5 the measured total rms fluctuating pressure level at the wall was 152 dB. This is 18 dB greater than what would be expected from turbulence alone, which suggests that the flow noise in the test section is dominated by acoustic sources external to the local microphone measurement region. More tests are planned to better understand the contributions to test section flow noise.

As already mentioned, acoustic waves are propagated from left to right, across the surface of the test specimen, and into a termination section designed to minimize reflections over the frequency range of interest. Two 6-mm, condenser-type microphones are flush mounted in the test section: one at the test specimen leading edge on the side wall and the other on an axial traverse bar, which forms a portion of the upper wall of the test section. A 13-mm-wide, precision-machined slot in the top wall of the flow impedance tube allows this axial traverse bar to traverse the test section length by means of a computer-controlled digital stepping motor. The data acquisition program automatically positions the traversing microphone at 34 preselected locations x_l, which range from 203 mm upstream of the leading edge to 50 mm downstream of the trailing edge of the test specimen. At each measurement location, a transfer function between the traversing and fixed microphones is measured and is used to determine the SPL (x_l) and phase $\phi(x_l)$ relative to the fixed microphone location. The complex acoustic pressure at the wall location is determined from the equation

$$p(x_l, H) = p_{\text{ref}} 10^{\frac{\text{SPL}(x_l)}{20}} e^{i\phi(x_l)} \tag{21}$$

where the reference pressure p_{ref} is 20 μPa.

The source-plane acoustic pressure and exit-plane impedance are functions of position along these planes. Therefore, transverse probe microphones should be used to measure these data when the test specimen is installed. This facility is not designed to easily accommodate transverse probe microphones because it is intended to operate below the cuton frequency of any higher-order modes. This experiment was, therefore, carefully designed to minimize higher-order mode effects along the source and exit planes. Almost all data for the duct propagation model were obtained from measurements made by the upper wall traversing microphone. Note that, because of the sound absorbing properties of the liner, high-order mode effects cannot be avoided in the liner region. Thus, high-order modes and reflections are generally present in the vicinity of the leading and trailing edges of the specimen.

To avoid the need for a transverse probe, the source plane was located 203 mm upstream of the leading edge of the test specimen in the hardwall section of the duct, and the source frequency was kept below the cuton frequency of higher-order hardwall modes. Higher-order mode effects caused by the installation of the test specimen are expected to decay upstream of the leading edge of the test specimen. Therefore, the source pressure at each point along the source plane is set to the value measured at the upper wall source location. A similar procedure is applied at the exit plane. The exit plane is located 203 mm downstream of the trailing edge of the test specimen, also in the hardwall section of the duct. The switched two-microphone method[13] was used to obtain the exit impedance. Almost identical exit impedance was measured for both the hardwall and the soft test liner configurations. Because the exit plane is 4 duct heights downstream of the trailing edge of the liner and higher-order modes are cut off, higher-order modes generated by the installation of the liner are not expected to carry appreciable acoustic energy to the exit plane. Thus, the exit impedance values at all points along the exit plane are set to that obtained at the side wall.

Impedance Eduction Technique

The measured data $p_s(y)$ and $\zeta_{\text{exit}}(y)$ provide a set of consistent boundary data for testing the impedance eduction technique. The solution to Eq. (18) gives the upper wall acoustic pressure as a function of the undetermined coefficients β_{Iq}. These coefficients are determined from the measured upper wall acoustic pressures. The procedure is to determine values of these coefficients such that the upper wall pressure solution obtained from Eq. (18) reproduces the measured upper wall acoustic pressures $p(x_l, H)$. Thus, we minimize the objective function

$$\psi(\beta_{Iq}) = \frac{1}{m}\sum_{l=1}^{m} |p(x_l, H) - P_{\text{FE}}(x_l; \beta_{Iq})| \qquad (22)$$

Note that this positive-definite objective function may be interpreted as the difference between the known acoustic wall pressure and that computed by the finite element method.

Because the optimization algorithm makes use of the objective function gradient to find its minimum and this function is available only in numerical form, i.e., as a finite element solution of Eq. (18), Stewart's adaptation of the Davidon–Fletcher–Powell optimization method is used to obtain the minimum.[14]

Description of Test Liners

The following section demonstrates the ability of the current method [grazing-incidence tube (GIT) method] to converge to the known normal incidence admittance of a solid steel plate and to the known normal incidence impedance of two soft test liners. The soft test liners were chosen because their impedances were shown to be fairly insensitive to the flow Mach number and SPLs.[15] Baseline impedance spectra for these two liners were established, therefore, from measurements in a normal-incidence tube (NIT). The three liners, shown schematically in Fig. 5, are intended for validation purposes only and are described in detail here.

1) There is a stainless-steel insert that continues the hardwall condition of the flow duct and provides a baseline condition for establishing zero admittance.

2) There is a ceramic structure of parallel, cylindrical channels, 0.635 mm in diameter, embedded in a ceramic matrix. The

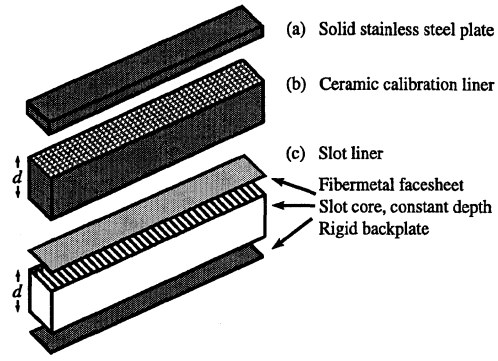

Fig. 5 Schematic of test liners.

83-mm-deep channels, i.e., $d = 83$ mm, separated by a wall thickness ranging from 0.1 to 0.2 mm, run perpendicular to the exposed surface to provide a surface porosity of 57% and resonant frequency of 1 kHz. The channels are rigidly terminated such that each is isolated from its neighbor to ensure a locally reacting structure. The channel diameter is small enough that the flow effects are minimal without the typical addition of a cover sheet.[15]

3) The final test liner is a 76-mm-deep, i.e., $d = 76$ mm, slot liner composed of 65 slot cavities with a resonant frequency of 1.15 kHz. The slot liner consists of 66 aluminum parallel plates that are placed approximately 6 mm apart. A 100 kg/m^2-s fibermetal facesheet is bonded to the surface of the liner.

Results and Discussion

Computer Code

An in-house computer code that implements the GIT impedance eduction method has been developed. Solution of the finite element matrix equation and the minimization of the objective function were performed by using highly developed software packages available at NASA Langley Research Center. Results are computed on a DEC-Alpha workstation. An evenly spaced 251×11 grid is used ($N = 251$ and $M = 11$) in the finite element discretization for all calculations. This grid ensures that a minimum of 10 elements per axial wavelength is used in the finite element discretization at the highest frequency of interest. Results are presented for six selected frequencies (0.5, 1.0, 1.5, 2.0, 2.5, and 3.0 kHz) and four target centerline Mach numbers (0.0, 0.1, 0.3, and 0.5). All calculations are performed at standard atmospheric conditions using the duct geometry of the NASA Langley Research Center Flow Impedance Tube Facility, i.e., $H = 51$, $L = 812$, $L_1 = 203$, and $L_2 = 609$ mm. The undetermined coefficients β_{Iq}, consistent with the measured acoustic pressure distribution on the upper wall, are returned by the GIT method. Note that all results are computed in terms of the admittance function $\beta(x)$; the corresponding impedance function is obtained from its reciprocal, i.e., $\zeta(x) = 1/\beta(x)$.

The objective function for all results given is constructed by using all 34 upper wall points, i.e., $m = 34$. It should be noted that the value of $\psi(\beta_{Iq})$ obtained at the minimum point was heavily dependent on the flow Mach number, frequency, and test liner construction. Recorded values at the optimum were in the range $10 \le \psi \le 600$. Generally, the smallest value of the objective function at the minimum point was obtained for the rigid test liner. No correlation between the magnitude of the error in the educed impedance or admittance and the value of the objective function at the minimum point was observed. Thus, the intuitive idea that smaller errors in the educed impedance or admittance values occur at low values of ψ was not supported by results in this study. Further, because all liners tested in this study have constant wall admittance functions β, the number of optimization variables was reduced from $8(N-1)$ to 2. This constant admittance function β is obtained from Eq. (14) by setting

$$\beta_{I2} = \beta_{I4} = 0 + 0i, \qquad \beta_{I1} = \beta_{I3} = \beta \qquad (23)$$

Thus, the wall objective function is a function only of the uniform admittance β, i.e., $\psi = \psi(\kappa, \sigma)$. Here, κ is the conductance and σ is the susceptance of the test liner, i.e., $\beta = \kappa + i\sigma$. Further, it is

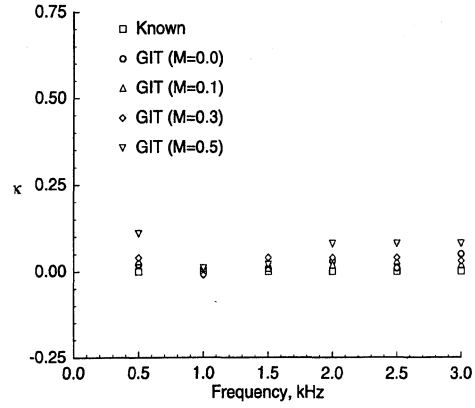

Fig. 6a Comparison of conductance spectra for rigid test liner.

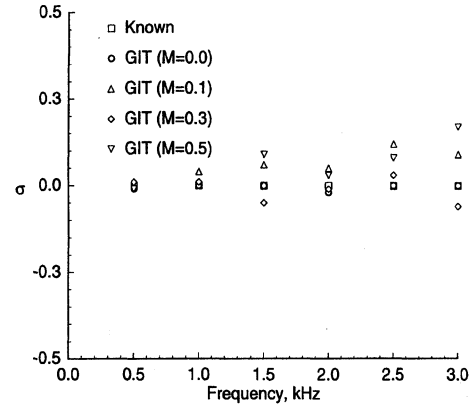

Fig. 6b Comparison of susceptance spectra for rigid test liner.

convenient to present results for the two soft liners in terms of the resistance θ and reactance χ of the test liner ($\zeta = \theta + i\chi$). Note that the admittance or impedance spectra computed for each flow Mach number consumed less than 12 min of CPU time on the workstation.

Rigid Test Liner

Figure 6 shows a comparison of the admittances educed in the grazing flow tube using the GIT method with the known values of a solid surface, i.e., conductance and susceptance values for a solid surface are zero. These comparisons are shown for each target centerline Mach number. GIT-educed conductance and susceptance values for this test liner not only are independent of the flow Mach number but are in excellent agreement with the known values of a solid surface. Note that the accuracy of the GIT-educed susceptance spectrum is slightly less than that of the GIT-educed conductance spectrum.

Ceramic Test Liner

Comparisons between the GIT-educed impedance spectrum and the NIT-educed spectrum for the ceramic test liner are shown in Fig. 7. These spectra agree reasonably well, except at 0.5 kHz and near the antiresonant frequency, i.e., 2.0 kHz, of the ceramic material. This poor result near antiresonance is typical for impedance-eduction techniques inasmuch as the liner appears acoustically hard, i.e., highly reflecting, to the aeroacoustic environment at that frequency. This hardness is supported by the computation of the admittance at 2.0 kHz, which gives a normalized conductance range of $0 < \kappa < 0.27$ and a normalized susceptance range of $-0.13 < \sigma < 0.10$. Note that Fig. 7 shows that the impedance spectrum is minimally influenced by the flow Mach number, except at the lowest frequency of interest, i.e., 0.5 kHz. The dependency of the impedance on the flow Mach number at 0.5 kHz was not expected and is still under investigation.

Note that for the ceramic test liner there is a slight trend toward divergence between the NIT- and GIT-educted impedance spectra as the flow Mach number increases (Fig. 7). As shown in Fig. 4,

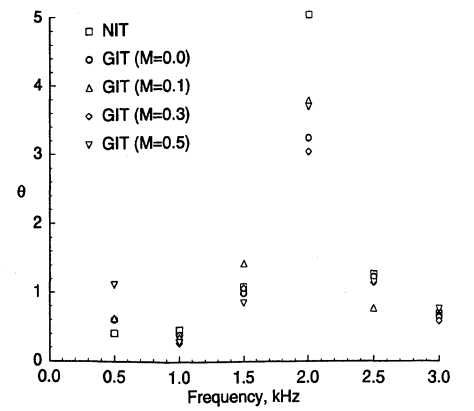

Fig. 7a Comparison of resistance spectra for ceramic calibration liner.

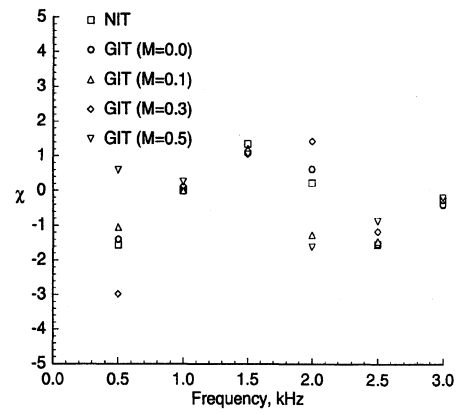

Fig. 7b Comparison of reactance spectra for ceramic calibration liner.

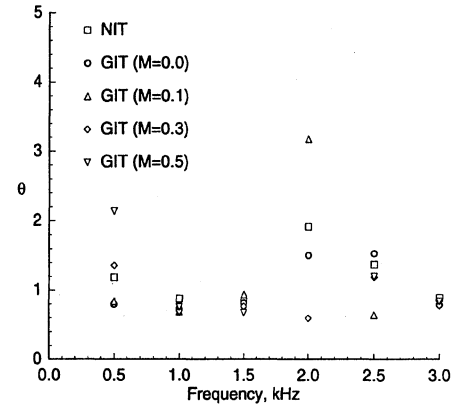

Fig. 8a Comparison of resistance spectra for slot liner.

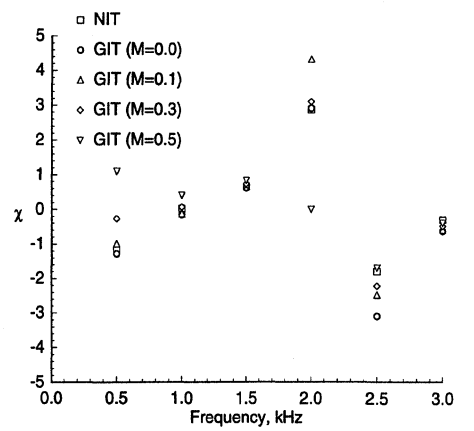

Fig. 8b Comparison of reactance spectra for slot liner.

the flow enters the duct sufficiently far upstream of the source plane that the duct wall shear layers, i.e., that are introduced by real flow effects, have nearly merged throughout the computational domain. Because the gradients in these shear layers increase with the flow Mach number, the uniform flow assumption is violated at the higher flow speeds. This accounts for the slight divergence between the NIT- and GIT-educed impedance spectra at the higher values of flow Mach number in Fig. 7. Thus, further minimizing this divergence will require the inclusion of mean flow gradients in the acoustic equations [see Eqs. (1–3)].

Slot Liner

Figure 8 shows comparisons between the NIT-educed impedance spectrum and the GIT-educed spectrum for the slot liner. For reasons mentioned earlier, a discrepancy is noted between the NIT- and GIT-impedance spectra at the frequency closest to the antiresonant frequency of the slot liner, i.e., 2.0 kHz. When compared in the admittance plane, however, the comparison between NIT- and GIT-educed results improved significantly ($0.06 < \kappa < 0.16$ and $-0.27 < \sigma < 0.00$). Otherwise, the agreement between the NIT- and GIT-educed impedance spectra is generally good. Again, the poor comparisons at a frequency of 0.5 kHz require further investigation.

Conclusions

On the basis of the results of this work, the following specific conclusions are drawn:

1) The current adaption of the Davidon–Fletcher–Powell optimization algorithm to the impedance-eduction method represents a significant step forward in impedance measurement technology in flow.

2) The GIT-educted results compare favorably with NIT-educed normal incidence admittance spectra for one rigid liner and with NIT-educed impedance spectra for two soft test liners in a uniform flow, except at the antiresonant frequency. Difficulties at antiresonant frequencies are typical in impedance/admittance-eduction methods.

3) The impedance of the soft test liners is also dependent on the flow Mach number at a frequency of 0.5 kHz. This dependency of the impedance on the flow Mach number at 0.5 kHz is unexpected and requires further investigation.

4) The success of the GIT impedance-eduction method warrants the extension of the method to include the refractive effects of the flow.

References

[1]Armstrong, D. L., Beckemeyer, R. J., and Olsen, R. F., "Impedance Measurements of Acoustic Duct Liners with Grazing Flow," 87th Meeting of the Acoustical Society of America, New York, April 1974.

[2]Watson, W. R., "A Method for Determining Acoustic-Liner Admittance in a Rectangular Duct with Grazing Flow from Experimental Data," NASA TP-2310, July 1984.

[3]Watson, W. R., "A New Method for Determining Acoustic-Liner Admittance in Ducts with Sheared Flow in Two Cross-Sectional Directions," NASA TP-2518, Oct. 1985.

[4]Watson, W. R., Tanner, S. E., and Parrott, T. L., "A Finite Element Model for Extracting Normal Incidence Impedance in Nonprogressive Acoustic Wave Fields," *Journal of Computational Physics*, Vol. 125, No. 1, 1996, pp. 177–186.

[5]Watson, W. R., Tanner, S. E., and Parrott, T. L., "Validation of a Numerical Method for Extracting Liner Impedance," *AIAA Journal*, Vol. 34, No. 3, 1996, pp. 548–554.

[6]Watson, W. R., Tanner, S. E., and Parrott, T. L., "Optimization Method for Educing Variable-Impedance Liner Properties," *AIAA Journal*, Vol. 36, No. 1, 1998, pp. 18–23.

[7]Kraft, R. E., "Theory and Measurements of Acoustic Wave Propagation in Multi-Segmented Rectangular Ducts," Ph.D. Dissertation, Dept. of Mechanical Engineering, Univ. of Cincinnati, Cincinnati, OH, May 1976.

[8]Myers, M. K., "On the Acoustic Boundary Condition in the Presence of Flow," *Journal of Sound and Vibration*, Vol. 71, No. 3, 1980, pp. 429–434.

[9]Chandrakant, S., and Abel, J. F., *Introduction to the Finite Element Method*, Van Nostrand Reinhold, New York, 1972, pp. 144, 145.

[10]Watson, W. R., "A Comparison of Continuously Varying Resistance and Cavity Depth Liners for Quieting Aircraft Engines," M.S. Thesis, School of Engineering and Applied Science, George Washington Univ., Washington, DC, May 1978.

[11]Schlichting, H., *Boundary-Layer Theory*, McGraw–Hill, New York, 1979, pp. 598–600.

[12]Parrott, T. L., and Jones, M. G., "Pressure Probe and Hot-Film Probe Responses to Acoustic Excitation in Mean Flow," NASA TP-2581, June 1986.

[13]Jones, M. G., and Parrott, T. L., "Evaluation of a Multi-Point Method for Determining Acoustic Impedance," *Mechanical Systems and Signal Processing*, Vol. 3, No. 1, 1989, pp. 15–35.

[14]Stewart, G. W., III, "A Modification of Davidon's Minimization Method to Accept Difference Approximations of Derivatives," *Journal of ACM*, Vol. 14, No. 1, 1967, pp. 72–83.

[15]Parrott, T. L., Watson, W. R., and Jones, M. G., "Experimental Validation of a Two-Dimensional Shear-Flow Model for Determining Acoustic Impedance," NASA TP-2679, May 1987.

M. Samimy
Associate Editor